SANDIA REPORT

SAND2014-18023
Unlimited Release
September 2014

Results from laboratory tests of the two-dimensional Time-Encoded Imaging System

Jim Brennan,
Erik Brubaker,
Mark Gerling,
Nathalie Le Galloudec,
Peter Marleau,
Kyle McMillan,
Aaron Nowack

Sandia National Laboratories

Prepared by Peter Marleau
Sandia National Laboratories
Albuquerque, New Mexico 87185 and Livermore, California 94550

Sandia National Laboratories is a multi-program laboratory managed and operated by Sandia Corporation, a wholly owned subsidiary of Lockheed Martin Corporation, for the U.S. Department of Energy's National Nuclear Security Administration under contract DE-AC04-94AL85000.

Issued by Sandia National Laboratories, operated for the United States Department of Energy by Sandia Corporation.

SAND2014-18023
Unlimited Release
September 2014

Results from laboratory tests of the two-dimensional Time-Encoded Imaging System

Jim Brennan
Erik Brubaker
Mark Gerling
Nathalie Le Galloudec
Peter Marleau
Kyle McMillan
Aaron Nowack

Radiation and Nuclear Detection Systems
Sandia National Laboratories
P.O. Box 969
Livermore, California 94551-MS9406

Abstract

A series of laboratory experiments were undertaken to demonstrate the feasibility of two dimensional time-encoded imaging. A prototype two-dimensional time encoded imaging system was designed and constructed. Results from imaging measurements of single and multiple point sources as well as extended source distributions are presented. Time encoded imaging has proven to be a simple method for achieving high resolution two-dimensional imaging with potential to be used in future arms control and treaty verification applications.

ACKNOWLEDGMENTS

This work was supported by NA-221, the office of non-proliferation R&D of the NNSA.

CONTENTS

FIGURES

TABLES

No table of figures entries found.

NOMENCLATURE

DOE	Department of Energy
HDPE	High Density Polyethylene
keVee	kilo-electronVolt electron equivalent
LS	Liquid Scintillator
MCNP	Monte Carlo N-Particle
MeVee	Mega-electronVolt electron equivalent
MLEM	Maximum Likelihood Expectation Maximization
PMT	Photomultiplier Tube
PSD	Pulse Shape Discrimination
RPM	Revolutions Per Minute
SNL	Sandia National Laboratories
SNM	Special Nuclear Material
TEI	Time Encoded Imaging
WGPu	Weapons Grade Plutonium

1.0. INTRODUCTION

We have developed a neutron detector system based on time-encoded imaging and demonstrated its applicability toward the spatial mapping of distributions of Special Nuclear Material (SNM). Other imaging methods require either multiple interactions (such as the Neutron Scatter Camera or Compton Imagers), leading to intrinsically low efficiencies, or spatial modulation of the signal (such as the Neutron Coded Aperture Imager (1)), which requires a complicated, high channel count, and expensive position sensitive detector. In contrast, a single detector using a time-modulated collimator can encode directional information in the time distribution of detected events. Time modulation as a means of directional discrimination, or imaging, has been an underexplored method for both gamma rays and especially high energy neutrons. This is the first investigation of two dimensional time-encoded imaging for nuclear nonproliferation applications.

We foresee two transformative advantages of time-encoded imaging. One is that a new design space is opened for effective and low-cost imaging systems. Time-encoding based imaging systems inherently have a low channel count, reducing cost and increasing robustness by simplifying system integration, calibration, and reducing systematic uncertainties. However in the case of two dimensional imaging, this comes at the cost of sensitivity. Effectively, the position sensitive detector of traditional coded aperture imaging systems is replaced by only one or a few independent single pixels causing a direct trade-off between the desired angular resolution and sensitivity of the imaging system which must be optimized toward an application.

The second advantage is that with time encoding, the angular resolution of the image reconstruction depends primarily on the collimator design. It is effectively decoupled from the method used for particle detection, which drives the detection efficiency as well as the energy resolution for gamma events. Thus in a time-encoding imager both angular resolution and energy resolution can be independently optimized.

Here we report the results of laboratory demonstrations of the time-encoded imaging concept applied to two-dimensional imaging of distributions of SNM with a prototype system. In Section 2.0 we describe the proof of feasibility prototype and its calibration. Sections 3.0 and 4.0 describe the measurements that were made and their analysis and results are presented in Section 5.0.

2.0. 2-D TIME-ENCODED NEUTRON IMAGING SYSTEM

As opposed to the task of source detection, the focus of the 2-D time encoded imaging prototype is to demonstrate proof of feasibility for high resolution image reconstruction. As such, the major driver has been in designing a mask-detector geometry that achieves a relatively high intrinsic angular resolution. The sensitivity and size of the scintillator detectors are secondary to the design of the mask. The final design shown in Figure 1 consists of 27 vertical rows of 149 - 1.9 cm wide x1.9 cm tall x 10 cm thick high density polyethylene (HDPE) mask elements with an inner radius of 45 cm giving an expected intrinsic angular resolution of ~2.5 degrees. Each row consists of eight - 1/8 arc sections machined from a single sheet of HDPE such that a 1/8" thickness on the inner radius remains as a backing to secure each element to each other.

The 8x27 = 216 segments are then adhered together to form a single self-supporting structure. An open fraction of 30% was determined to be optimal for the extended source distributions that were used in laboratory tests (2). There are therefore a total of 2816 mask elements. As the mask is rotated around two central 1" diameter x 1" deep liquid organic cells, the direction of any sources present are uniquely imprinted on their count rates as a function of time. Each cell is coupled to a Hamamatsu H1949-50, 2" diameter photomultiplier tube. Signals from the PMTs are digitized by a Struck SIS3316 16 channel 250 MHz desktop digitizer (3).

The mask pattern was determined using a pseudo random optimization in which 100 patterns were randomly produced and their simulated image reconstruction performance was evaluated against several test distributions. The mask with the most accurate reconstruction with the fewest artifacts was selected. The result is a far from optimized, but deemed good enough to demonstrate the feasibility of this technique.

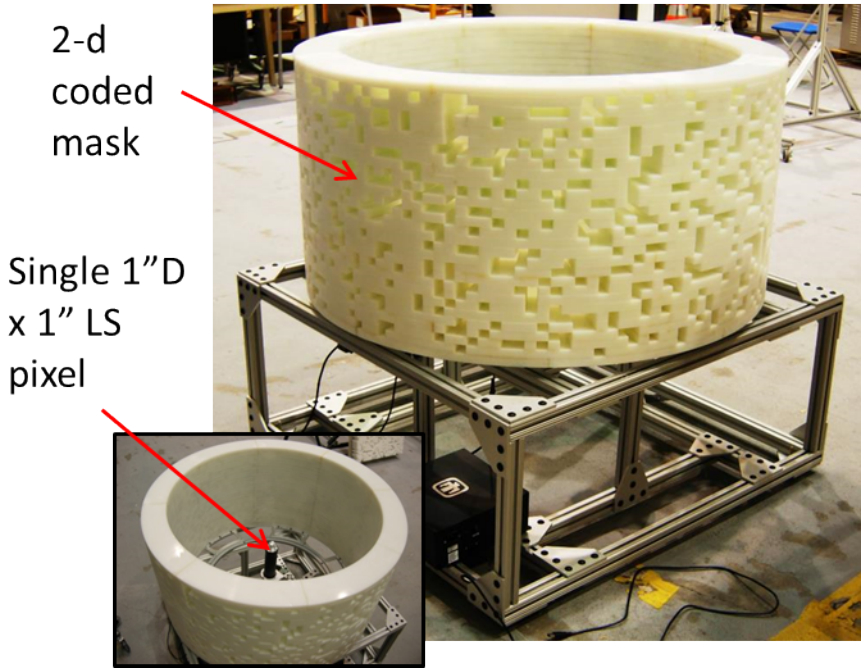

Figure 1 – Photograph of the 2-D time-encoded imager. Two central 1" diameter x 1" thick liquid organic scintillator detectors (seen in inset) are surrounded by a rotating high density polyethylene mask.

2.1. Calibrations

The Compton pulse height spectrum from a ^{22}Na gamma-ray source is used to match the gains of each PMT of the two central 1" diameter x 1" thick LS cells as seen in Figure 2. Further, the spectrum is fit using a Monte Carlo spectrum and energy smearing. This provides a measure of the gain and energy resolution that can be used in Monte Carlo simulations of the detector response.

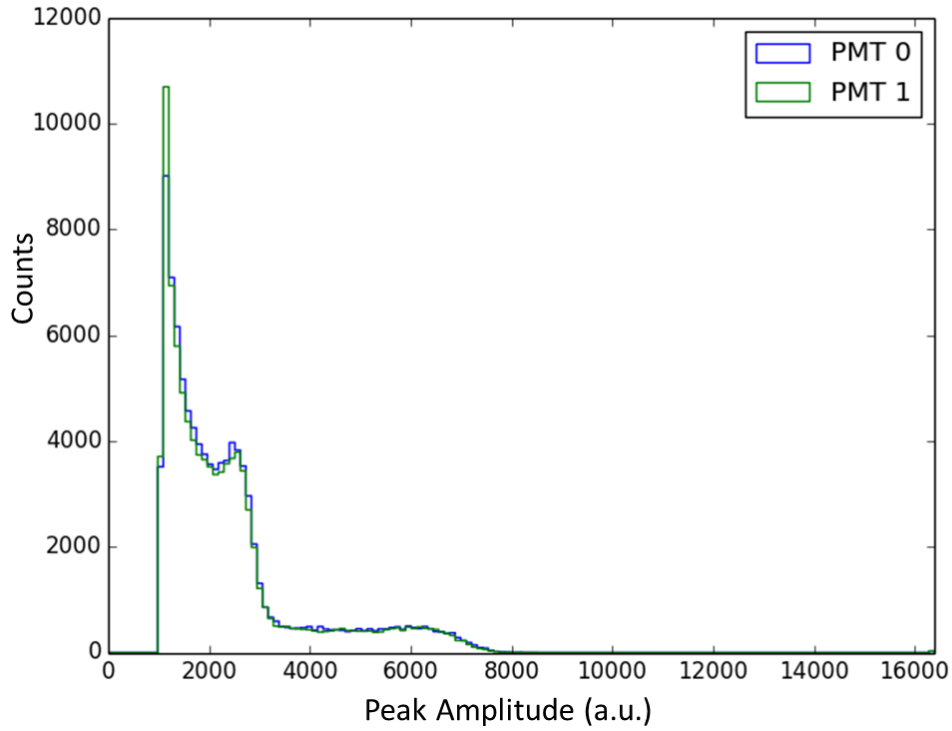

Figure 2 – The measured pulse height spectrum from the two LS cells using a ^{22}Na gamma source.

Next, calibrations measurements were obtained using a ^{252}Cf fission source in order to establish neutron/gamma discrimination cuts based on pulse shape. Figure 3 shows an example of the one such calibration for each of the two LS cells. A pulse shape discrimination (PSD) parameter is defined as the ratio of a tail integration to a total integration of the sum. This is then plotted against the pulse height and a pulse height dependent cut is determined. The cut used in this work is based on the requirement that each event have greater than 5 sigma significance (99.999% probability) of being a neutron and not a gamma-ray.

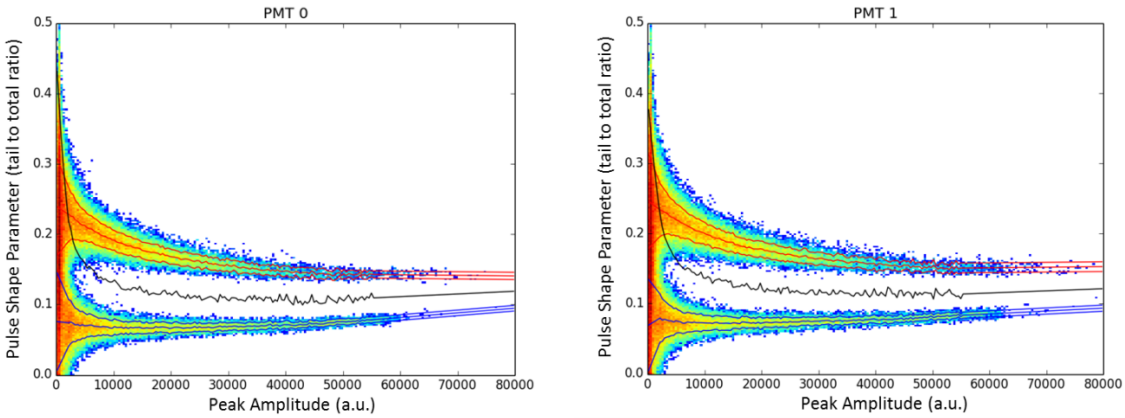

Figure 3 – The measured pulse shape parameter vs. pulse height for the two LS cells. Neutron/proton recoils lie within the upper band defined by the red lines (middle red line is the mean and top and bottom red lines contain 3 sigma deviations from the mean) while gamma/electron recoils fall in the lower band defined by the blue lines (middle blue line is the mean and top and bottom blue lines contain 3 sigma deviations from the mean). The black line between the two distributions represents the division between >99.999% probability of being neutron.

3.0. MEASUREMENTS

For all measurements presented in this work one or more matched 35 microCurie Cf252 fission sources were placed 2.0 meters from the center of the imaging system. In the point source measurements, the Cf252 sources were held in a stand that allowed their horizontal and vertical positions to be continuously varied.

The ring source was physically approximated by rotating a single Cf252 point source in a circle using an automated rig with its axis oriented toward the center of the imaging system. The source was set to rotate with a period that was a non-integer fraction of the mask rotation period such that given a long enough dwell time, all combinations of source location and mask orientation would be sampled. For some of the shorter dwell times presented below, this is not guaranteed, however it is expected to be a close enough analog to a continuous extended source distribution for these tests.

During the measurements the detector system continuously buffers data within the SIS3316 digitizers. Because the trigger rates in the LS cells are quite low (a few Hz), hours of data can be buffered. After a fixed dwell time, the detector is halted and the entire buffer is written to hard disk. This allows for close synchronization of positional information recorded by the encoder to the data recorded for each time period without having to use multithreaded acquisition software. However, because of this decision, the system maintained a small dead-time of ~5% during read out. In future iterations of this system, multithreaded data acquisition software will eliminate this dead-time

As a preliminary test that the encoder positions were accurately mapped to the expected mask orientation, a Cf252 source was placed 1 cm from the mask at a height corresponding to a randomly chosen mask row. A comparison of the measured neutron rate modulation as

compared to the expected modulation pattern is shown in Figure 4. This provides confidence that the mask alignment and encoder synchronization is accurate.

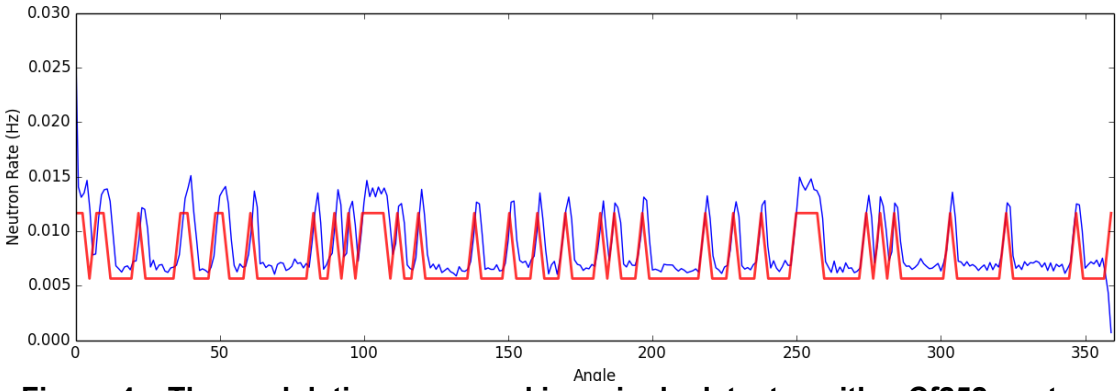

Figure 4 – The modulation measured in a single detector with a Cf252 neutron point source 1 cm from one row of the mask (blue) overlaid with the expected modulation pattern (red).

4.0. ANALYSIS

Raw data is first preprocessed: pulses are converted into a measure of the energy deposited (in MeVee) and a pulse shape parameter is extracted based on the ratio of the integral of a tail region of the pulse to the total charge integral. This parameter is then used to estimate the probability that each event is a neutron vs gamma-ray interaction based on the calibrations described in Section 2.1. Each event is time sorted and matched to a rotation angle based on the time stamp of the event and a time tagged list of encoder positions.

The result of preprocessing is two arrays (or histograms) of neutron counts vs. rotation angle, one for each LS detector. This is corrected for the time spent at each rotation angle and converted into neutron rates vs. rotation angle. Due to uneven amounts of time spent accelerating and decelerating as well as slippage in the drive wheels, the dwell time as a function of rotation angle frequently is not flat.

Lastly, these neutron rates vs. rotation angle are unfolded to produce a two-dimensional image using the Maximum-Likelihood Expectation-Maximization (MLEM) (4) algorithm. In this method, a detector response matrix is used to forward project an assumed neutron source distribution over the two-dimensional space to a predicted set of neutron measurements. The algorithm then provides an update to the source distribution based on a comparison between the measured and forward projected values. Each iteration of this updating procedure is statistically guaranteed to increase the likelihood that the source distribution produces the measured rates.

The detector response matrix is constructed using MCNP-PoliMi (5) simulations of neutrons transported through the HDPE mask as a function of azimuthal and vertical positions. Both the detector response matrix calculations and MLEM iterative reconstruction were implemented using CUDA to utilize parallelization on GPU processors (6).

5.0. RESULTS

In the following sections, the results of MLEM iterative image reconstructions are shown. The number of iterations that were used depended on the statistics found in each data set. With higher neutron counts, more iterations are possible before the statistical and systematic uncertainties found in the detector response matrix begin to amplify random fluctuations in the data to create imaging artifacts. The number of iterations is chosen based on the variance of background regions of the image. Near the ideal number of iterations (where the true likelihood will begin oscillating due to noise in the response matrix), the flat field background variance will steeply increase. In this work, the number where this occurs was selected by expert user intervention. Future work will include the automation of exit criteria in the MLEM algorithm.

Due to the cylindrical geometry of the TEI system, it is capable of imaging in an entire 360 degree field of view. However, in all of the following sections, we have limited the reconstruction to the portion of the field of view in which it was known that the source is present. We found that this did not significantly alter the final reconstructed image, but it allowed us to reduce the size of the detector response matrix and corresponding time to reconstruct the images. In this work we did not investigate the effect that radiation sources in other regions of the field of view would have on the ability to reconstruct the sources of interest.

5.1. Single point source

With mask modulation and registration established as discussed in Section 3.0, the point source response of the TEI system was explored. Figure 5 shows the MLEM reconstructed image of a single Cf252 point source at 2.0 meters in a 15 hour measurement. The FWHM of this image is smaller than its 1 degree binning. A similar level of performance was achieved with the Fast Neutron Coded Aperture Imager in a few 10s of minutes. However, with 1600 – one centimeter pixels in its position sensitive detector, the coded aperture system has 160 times the physical detector area. If the dwell time were to be corrected by equal neutron counts as a point of comparison, this 15 hour measurement is equivalent to ~5.6 minutes of a coded aperture measurement. Therefore, there are hints that, due to the simplicity of the TEI system, better performance per unit neutron can be achieved due to a reduction in systematic uncertainties.

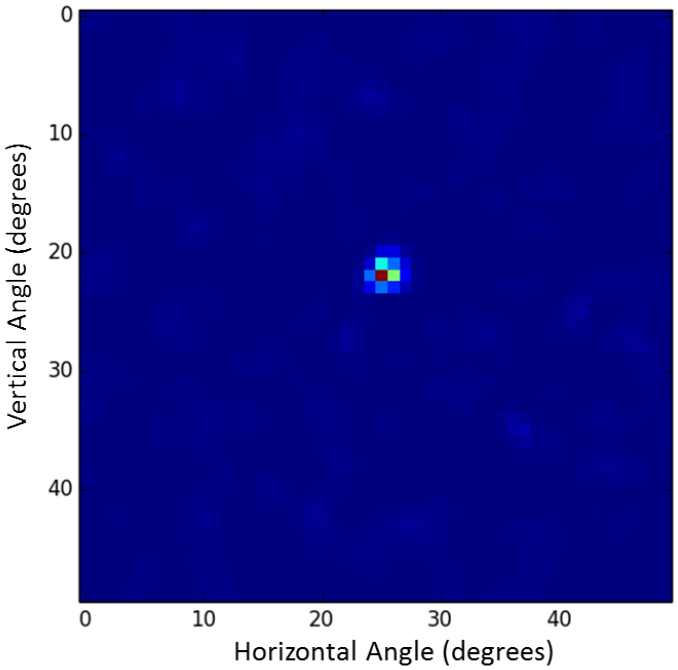

Figure 5 – MLEM reconstructed image of a single Cf252 neutron source at a distance of 2.0 meters with 15 hour dwell time.

5.2. Two point source resolution

In the second series of measurements, the TEI system's ability to resolve two point sources at varying angular separations is investigated. The MLEM reconstructed images shown in Figure 6 demonstrate that the resolvable angular separation achievable in 1 hour is less than 5 degrees. Considering that the expected intrinsic (geometric) angular resolution of the system is half this source separation (~2.5 degrees), this is a remarkable result.

In Figure 7 the limits of low angle separation are explored. Two point sources separated by only 2 degrees are reconstructed with 2 and 24 hour measurement times. In two hours the reconstructed image of two point sources is not significantly different than a single point source with twice the strength. However, in 24 hours the statistics are high enough that, though the image does not reveal two well separated sources, it is significantly different than a single point source (compare to Figure 5). Consistent with the discussion started in Section 5.1, this is another indication that the systematic variation and uncertainty in the TEI system is low.

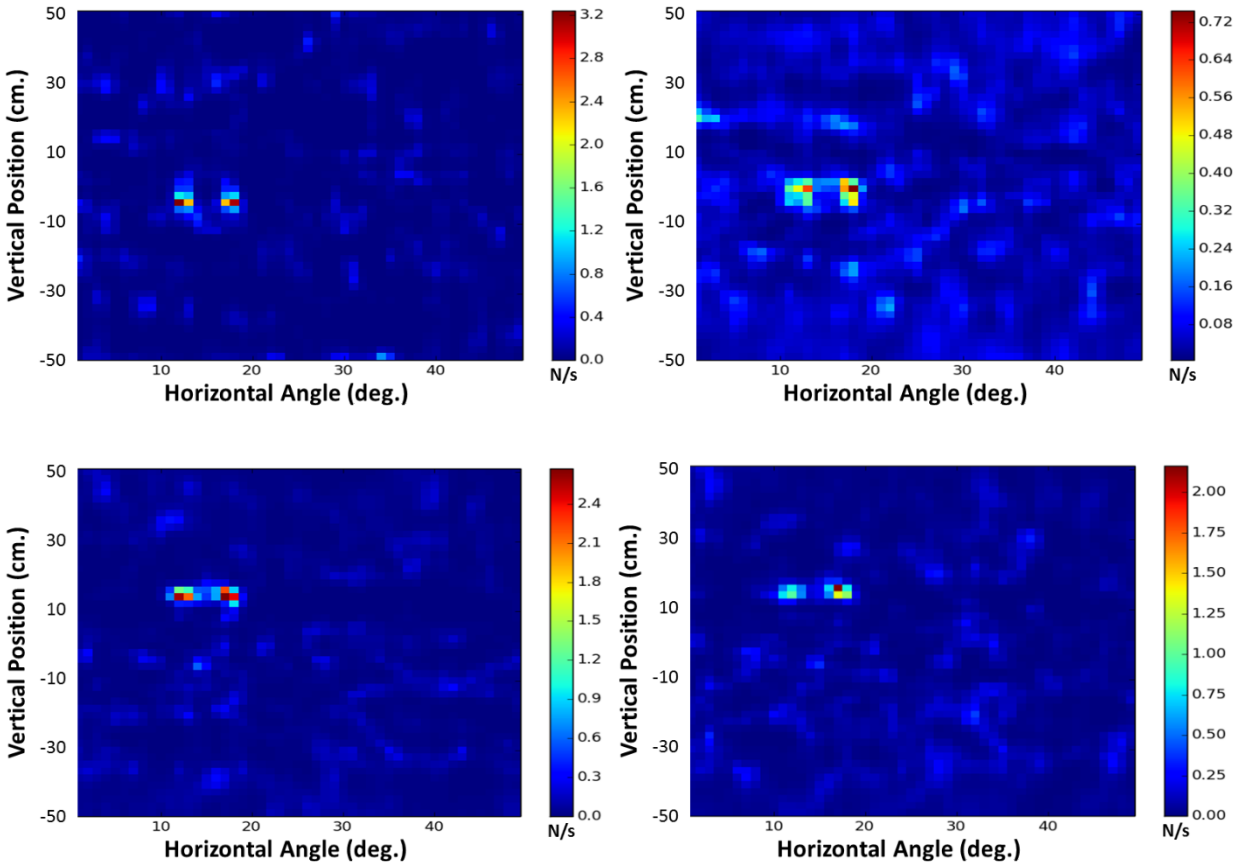

Figure 6 – MLEM reconstructions of two Cf252 neutron point sources separated by 5 degrees at 2.0 meter stand-off. (Left column) Sources at two different vertical positions (12 hours, 250 MLEM iterations). (Right column) Sources at the same positions as in the left column, but only 1 hour dwell (50 MLEM iterations).

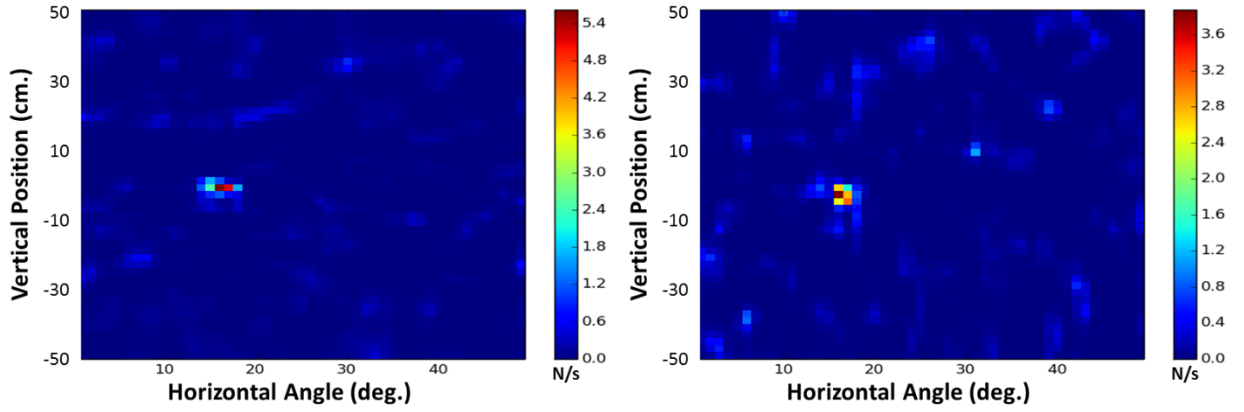

Figure 7 – MLEM reconstructions of two Cf252 neutron point sources separated by 2 degrees at 2.0 meter stand-off. (Left) 24 hour dwell time and 250 MLEM iterations. (Right) Same positions as on the left, but only 2 hour dwell time and 100 MLEM iterations.

5.3. Ring source

One property of coded aperture imaging is that the signal to noise decreases as multiple and/or extended sources are introduced (7) (8). Statistically, the signal from one source (or region of an extended source) contributes to the noise for another source (or other region of an extended source). In addition, the source strength is spread out over a larger fraction of the field of view so the intrinsic contrast to background will be worse. Therefore, extended source imaging is much more difficult and requires higher statistics to achieve.

To demonstrate the extended source imaging capability of the TEI system, a series of measurements using the Cf252 ring source described in Section 3.0 were conducted. In Figure 8 the MLEM image reconstructions for two different vertical displacements of the ring source are shown. Scaled by physical area, these measurements are approximately equivalent to 30 minutes of Neutron Coded Aperture Imager dwell time and similar imaging performance is achieved. In order to get a sense for how the images develop as a function of dwell time, we show the reconstructed images for three different times in Figure 9. It can be seen that something on the order of 12 hours is sufficient.

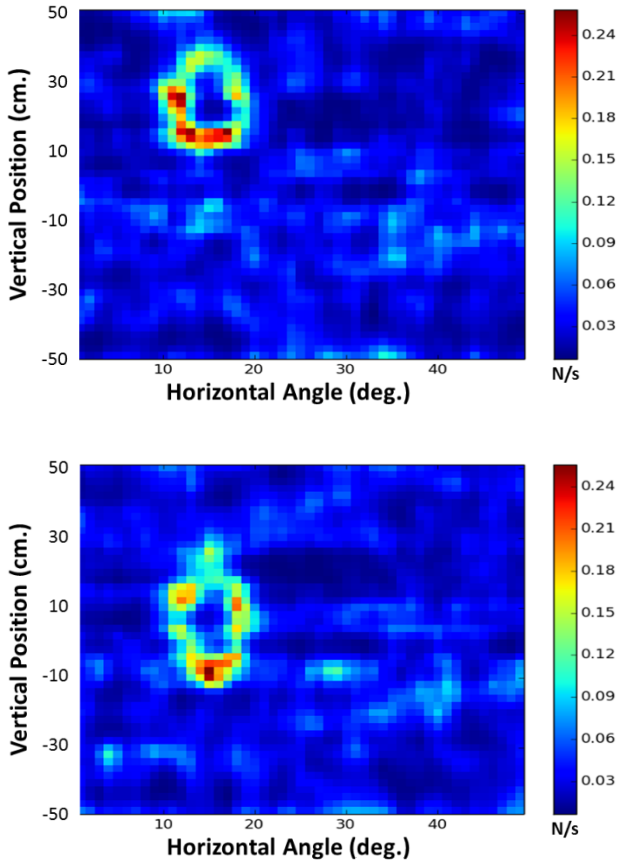

Figure 8 – MLEM reconstruction of a Cf252 ring source in two different locations at 2.0 meter stand-off. The color scale is in units of neutron rate (n/s). 94 hour dwell,100 MLEM iterations (bottom) and 72 hour dwell, 100 MLEM iterations (top). The apparent angular diameter of the source is expected to be 8.7 degrees. The color scale is in units of neutron rate (n/s).

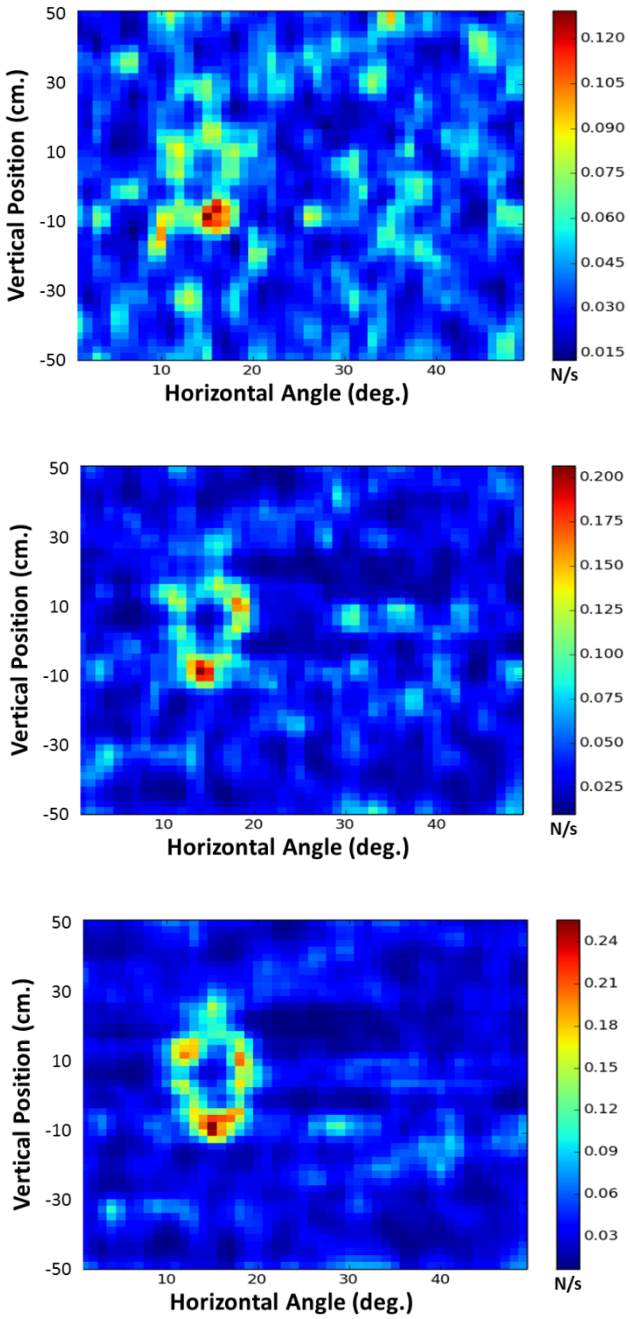

Figure 9 – MLEM reconstruction of the same ring source with different dwell times. (Top) 3 hours, 20 MLEM iterations, (middle) 12 hours, 50 MLEM iterations, (bottom) 72 hours, 100 MLEM iterations.

One issue that became apparent in creating these images is that because of the nature of the cylindrical geometry of the mask, there are artifacts that emerge as horizontal stripes in the reconstruction. We believe that there are four possible (conspiring) reasons for this:

1. Horizontally, the modulation is achieved through continuous rotation of the mask and therefore lends itself to a smooth reconstruction. Vertically, variations in the mask row to row can lead to different performance for different horizontal bands across the field of view of the imager.
2. Not every row of the mask pattern has the same open fraction. Therefore different horizontal bands in the field of view may have different efficiencies.
3. Different rows of the mask will have their own independent modulation performance. Since the mask was not well optimized, some rows may perform better than others.
4. For regions of the field of view with a line of site to the LS detectors that split two mask rows, the average modulation will be quite poor. For these regions one would expect to find on average one mask element and one aperture at any given rotation angle. Therefore the modulation will be weak.

In future research, these points can potentially be resolved (respectively):

1. Point 1 could potentially be addressed by changing to a spherical geometry without a single fixed rotation axis. However, such a mask would be difficult to engineer.
2. Point 2 could be addressed with a better optimized mask, but can also be corrected for by dividing out the vertical dependence of the efficiency. This was not done in this work.
3. Point 3 could be addressed optimizing the mask through a heuristic processes that converges toward best performers.
4. In Point 4, we understood that this would be a problem in designing this system and therefore added a second LS detector with vertical separation of an integer number plus one half the height of a mask element. This was done such that there would not be regions of the FOV that had this modulation problem for both detectors simultaneously. It is conceivable that a detector with vertical position resolution, such as a bar type geometry with a PMT on each end, could bring continuity to the reconstruction vertically.

6.0. CONCLUSIONS

Through a series of laboratory measurements on a variety of test objects, we have successfully demonstrated the feasibility of two-dimensional fast neutron imaging using the time encoded modulation of rates on a single pixel detector. Sub-degree resolution of a single point source and 2 degree separation resolution of two point sources in 12 hours was achieved. Extended source distributions were also successfully imaged and some performance issues along with a discussion of possible solutions were presented in Section 5.3.

Finally, in Figure 10 we provide a side by side visual comparison of images from the Fast Neutron Coded Aperture Imager (left) and the TEI system (right). The source strengths and expected distributions are similar. It is apparent that due to the much smaller physical detector size of the TEI system, longer dwell times are required. However, because of the simplicity of the TEI design, there is much less systematic uncertainty in the detector response resulting in a lower required dwell time than a simple scaling of physical areas.

The simplicity of analyzing a single time dependent neutron rate from a single neutron detector may also make this an attractive option for future arms control applications. This lends itself well to real time updating algorithms that could potentially operate behind an information barrier if one were deemed necessary.

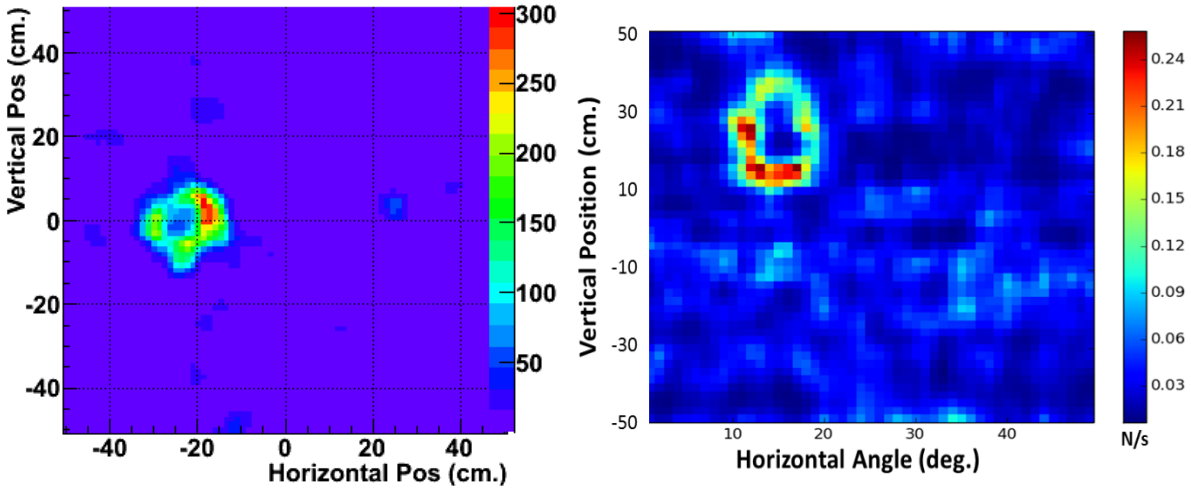

Figure 10 – MLEM reconstructed images from imaging studies using the ORNL/SNL Fast Neutron Coded Aperture Imager with 1 hour dwell time (left) and the two-dimensional Time Encoded Imager with 72 hour dwell time (right).

7.0. REFERENCES

1. *Fast Neutron Coded-Aperture Imaging of Special Nuclear Material Configurations.* **Hausladen, P., Blackston, M., Brubaker, E., Chichester, D., Marleau, P., Newby, J.** 2012. INMM Anual Meeting.
2. *High Resolution Imaging of Fission Energy Neutrons.* **Marleau, P., Blackston, M., Brennan, J., Brubaker, E., Gerling, M., Hausladen, P., McMillan, K., Mrowka, S., Newby, J.** 2012. INMM Annual Meeting.
3. **Struck.** SIS3316 manual. [Online] 2013. http://www.struck.de/sis3316-2013-06-24.pdf.
4. *Maximum Likelihood Reconstruction for Emission Tomography.* **Shepp, L.A., Vardi, Y.** 2, October 1982, IEEE Transactions on Medical Imaging, Vol. 1, pp. 113-122.
5. **Padovanni, E., Pozzi, S.A., Clarke, S.D., Miller, E.C.** *Introduction to MCNPX-PoliMi Version 2.7.* 2012.
6. **Nickolls, J., Buck, I., Garland, M., Skadron, K.** Scalable Parallel Programming with CUDA. *Queue GPU Computing.* 2008, Vol. 6, 2.
7. *Coded Aperture Imaging with Uniformly Redundant Arrays.* **Fenimore, E.E., Cannon, T.M.** 3, 1978, Applied Optics, Vol. 17.
8. *Coded Aperture Imaging in X- and Gamma-Ray Astronomy.* **Caroli, E., Stephen, J.B., Di Cocco, G., Natalucci, L., Spizzichino, A.** 1987, Space Science Reviews, Vol. 45, pp. 349-403.
9. *Time-encoded imaging of energetic radiation.* **Brennan, J., Brubaker, E., Gerling, M., Marleau, P., Nowack, A., Schuster, P.** San Diego, CA : s.n., 2013. Proc. SPIE 8852, Hard X-Ray, Gamma-Ray, and Neutron Detector Physics XV. 885203.

DISTRIBUTION

1	MS9406	Erik Brubaker	8127
2	MS9406	Scott Kiff	8127
3	MS9406	Peter Marleau	8127
4	MS9406	Melinda Sweany	8127
5	MS9406	Craig Tewell	8127
6	MS9292	Ken Patel	8125
7	MS9291	Jim Brennan	8125
8	MS9291	Dan Throckmorton	8125
9	MS9014	Nathalie Le Galloudec	8127
10	MS9004	Wen Hsu	8120
11	MS9004	Jim Lund	8130
12	MS1374	Kevin Seager	6831
13	MS1374	Sharon Deland	6831
14	MS0968	Robert Tachau	5753
15	MS0899	Technical Library	9536 (electronic copy)


Sandia National Laboratories